2010

Myosin Light Chain Kinase Mediates Transcellular Intravasation Of Breast Cancer Cells Through The Underlying Endothelial Cells: A Three-Dimensional Fret Study

S. Khuon

L. Liang

R. W. Dettman

P. H. S. Sporn

R. B. Wysolmerski

See next page for additional authors

Myosin light chain kinase mediates transcellular intravasation of breast cancer cells through the underlying endothelial cells: a three-dimensional FRET study

Satya Khuon[1,2], Luke Liang[1], Robert W. Dettman[3], Peter H. S. Sporn[4,5], Robert B. Wysolmerski[6,7] and Teng-Leong Chew[1,2,*]

[1]Cell Imaging Facility, [2]Department of Cell and Molecular Biology, [3]Department of Pediatrics and [4]Division of Pulmonary and Critical Care Medicine, Department of Medicine, Northwestern University Feinberg School of Medicine, Chicago, IL 60611, USA
[5]Jesse Brown Veterans Affairs Medical Center, Chicago, IL 60612, USA
[6]Department of Neurobiology and Anatomy and [7]The Mary Babb Randolph Cancer Center, West Virginia University School of Medicine, Morgantown, WV 26506, USA
*Author for correspondence (t-chew@northwestern.edu)

Accepted 18 November 2009
Journal of Cell Science 123, 431-440 Published by The Company of Biologists 2010
doi:10.1242/jcs.053793

Summary

The transient and localized signaling events between invasive breast cancer cells and the underlying endothelial cells have remained poorly characterized. We report a novel approach integrating vascular engineering with three-dimensional time-lapse fluorescence resonance energy transfer (FRET) imaging to dissect how endothelial myosin light chain kinase (MLCK) is modulated during tumor intravasation. We show that tumor transendothelial migration occurs via both paracellular (i.e. through cell-cell junctions) and transcellular (i.e. through individual endothelial cells) routes. Endothelial MLCK is activated at the invasion site, leading to regional diphosphorylation of myosin-II regulatory light chain (RLC) and myosin contraction. Blocking endothelial RLC diphosphorylation blunts tumor transcellular, but not paracellular, invasion. Our results implicate an important role for endothelial myosin-II function in tumor intravasation.

Key words: FRET imaging, Cytoskeletal signaling, Endothelium, Transcellular invasion, Tumor intravasation, Vascular engineering

Introduction

The endothelial barrier presents a key rate-limiting step against invasive tumor cells during metastasis (Zijlstra et al., 2008). Once that barrier is breached, the tumor cells will enter the blood stream, through which they are rapidly dispersed to distant sites where they can colonize and establish secondary tumors. The endothelium has been conventionally considered as an important line of defense against tumor dissemination, in that the endothelial barrier greatly reduces invasion rate (Wittchen et al., 2005). Several recent findings, however, have established a novel paradigm in which endothelial cells play significant roles in the invasiveness of cancer cells. First, breast cancer cells exhibit increased rate of dispersion and clearance through hematogeneous dissemination the closer they are located to a blood vessel (Kedrin et al., 2008). Second, the invasive potentials of several cancer cell lines have been shown to be endothelial-cell-dependent (Mierke et al., 2008b). Although the process of tumor invasion has been the subject of intense investigation, the actual molecular mechanisms of tumor transendothelial migration remain poorly understood.

The physical process of tumor intravasation involves the interaction of at least two cell types: the invading tumor and the opposing endothelial cell, and will engage the mechano- and chemico-transduction properties of the cytoskeleton of the two adjacent cells. To decipher the highly transient and localized tumor-mediated signals in the endothelial cells, we have devised a three-dimensional (3D) assay with which we can examine the real-time intra-endothelial signaling events, as modulated by the invading tumor cell. This highly adaptive assay involves the engineering of vasculature network in a 3D collagen matrix using endothelial cells that express a fluorescent resonant energy transfer (FRET)-based biosensor that will report the activity of myosin light chain kinase (MLCK) in the cell in real-time (Chew et al., 2002). We could demonstrate that the endothelial cells retain their ability to perform mechano-sensing in the collagen matrix. More importantly, the 3D collagen matrix environment induced extensive lumen formation, as confirmed by confocal and electron microscopy. The endothelial cells also showed basal-apical polarity in the correct orientation, as characterized by deposition of α4 laminin.

Using the 3D FRET-based invasion assay, we have characterized how the invading tumor modulates the MLCK-mediated actomyosin function in the underlying endothelium. We show that tumor cells are capable of transmigrating via either transcellular (i.e. through individual cells) or paracellular (i.e. though cell-cell junctions) routes. During transcellular invasion, the invading tumor cell triggers MLCK activation in the endothelial cell. This MLCK activity correlates with increased regional phosphorylation of myosin-II regulatory light chain (RLC) and localized endothelial myosin contraction. Using endothelial cells expressing RLC mutant that cannot be phosphorylated, we demonstrated that MLCK-mediated endothelial contractility played a key determining role in the mechanism of tumor intravasation.

The FRET-based tumor invasion assay provides an environment for endothelial cells to form vasculature wherein force generation can take place in 3D physiological milieu. Using this novel assay, we have shown that: (1) invading tumor cells, much like leukocytes, are capable of undergoing transcellular migration; (2) tumor cells induce

Journal of Cell Science

transient and regional MLCK activation and myosin contraction at the site of invasion; and (3) the transcellular invasion route is dependent on phosphorylation of myosin-II RLC. These results highlight the active role of endothelial cells in tumor intravasation.

Results

Engineering an in vitro 3D vascular network

Endothelial cells are sensitive mechanosensors whose biological responses include detecting and modulating subtle hemodynamic changes as well as isometric tension. To create a platform with which we could study the endothelial intracellular signaling during tumor invasion, we sought to generate a vascular network that better mimicked the physiological condition wherein endothelial cells were exposed to 3D extracellular matrix architecture and thus 3D isometric tension. Supplementary material Fig. S1A,B shows the schematic of 3D gel assembly suitable for live cell imaging. The endothelial cell-collagen gel mixture was cast within a porous polyethylene ring centered on top of a coverslip for confocal imaging. To assess the degree of free fluid exchange in the gel, CellTrace Oregon Green, a non-specific cell indicator dye, was added on top of the gel and the penetration rate of the dye was monitored upward from the bottom by confocal microscopy (supplementary material Fig. S1C). The dye stained the endothelial vascular network to near saturation level within 5 minutes. Further incubation to 10 minutes led to no discernible increase in fluorescent intensity, indicating that there was a rapid and free exchange of liquid, even at the very bottom of the gel where all subsequent imaging experiments in this study would be conducted.

Endothelial cells maintain their mechano-sensing capability in the 3D collagen matrix

Endothelial cells formed an extensive 3D vascular network in our collagen gels 24-30 hours following gel assembly (Fig. 1A,B). Calf pulmonary artery endothelial (CPAE) cells, human umbilical vein endothelial cells (HUVECs) and human microvessel endothelial cells formed equally extensive network under these assay conditions (data not shown).

To test whether endothelial cells maintained their ability to detect mechanical force, we characterized the 3D architecture of the vascular network under culture conditions with compromised isometric tension or in collagen gel exposed to persistent isometric tension. Cultured endothelial cells typically express 20-40 dynes of constitutive tension (Goeckeler and Wysolmerski, 1995), and this isometric tension is crucial in vascular development and maturation (Ingber and Folkman, 1989a; Ingber and Folkman, 1989b; Korff and Augustin, 1999). To abrogate the isometric tension detected by the embedded endothelial cells, the freshly solidified collagen was removed from the casting unit and suspended by its natural buoyancy in liquid medium. As shown in Fig. 1C, the formation of the vascular network was severely stunted in the absence of isometric tension, suggesting that the endothelial cells in the 3D matrix maintain their ability to respond to isometric force.

The 3D vascular network undergoes lumenization and establishes basal-apical polarity

To determine the formation of lumenized network in the 3D collagen gel, we performed confocal microscopy directly on the CellTrace-Oregon-Green-labeled endothelial cells in the unfixed

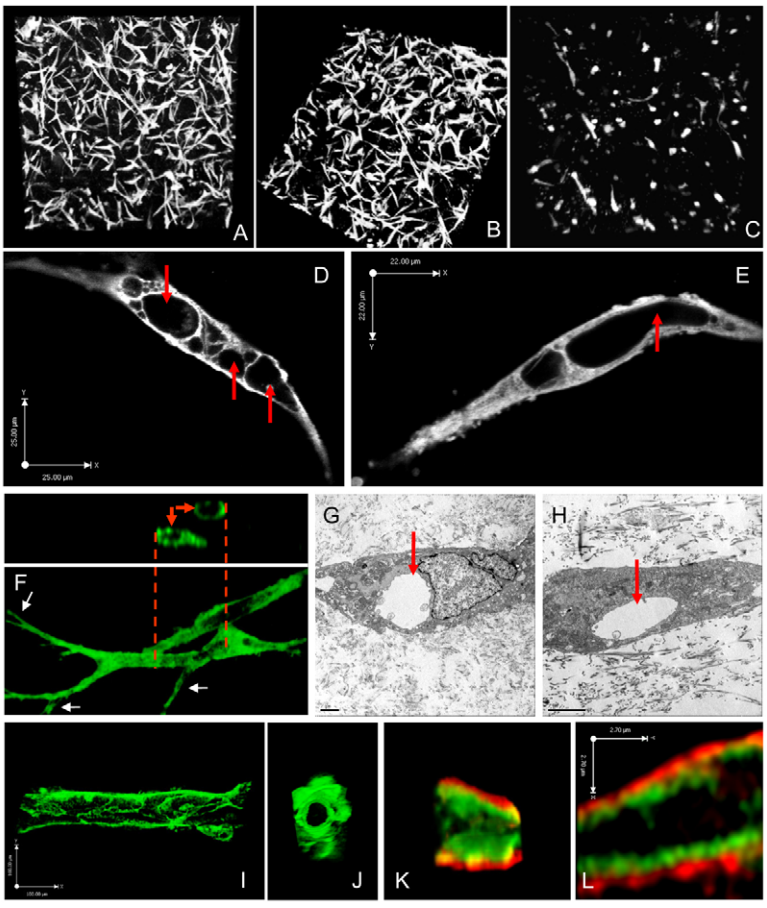

Fig. 1. Polarized endothelial cells maintain their mechano-sensing capability and form an interconnected and lumenized 3D vascular network in collagen gel matrix. (**A**) Confocal micrographs of endothelial cells forming an extensive vascular network 2 days after 3D gel assembly. (**B**) 3D reconstruction of the vascular network, tilted at an angle to highlight the multilayered nascent vascular tubes. (**C**) Absence of vascular network in the 3D gel with compromised isometric tension development. (**D**) Confocal optical section through a nascent vessel 24 hours after gel assembly. Note the number of vacuoles accumulating in the endothelial cell (red arrows). The vacuoles are of various sizes and separated by septum in the cytoplasm. (**E**) Confocal image of a vessel 2 days after gel assembly shows vacuoles gradually coalesced to form continuous lumen (red arrows). (**F**) At 3 days after gel assembly, endothelial cells establish a mature 3D vascular network with well-formed lumen and also show extensive sprouting (white arrows). The orthogonal view of the region indicated by the red dotted line shows the formation of lumen, as indicated by the red arrows. This network was constructed using endothelial cells expressing the MLCK FRET sensor, shown here in monochrome green. (**G**,**H**) Electron micrographs show the formation of lumen devoid of extracellular matrix components (red arrows). Scale bars: 1 µm. (**I**,**J**) Confocal micrographs showing the lateral and cross-sectional view of a single lumen extending through multiple cells in the 3D vascular network. Cell-cell border is marked by VE-cadherin immunostaining. Arrow in each direction represents100 µm. (**K**,**L**) Confocal 3D reconstructions showing endothelial cell (green) and α4 laminin (red) deposited at the periphery of the vascular system. The reconstructed image was digitally dissected to show the lumen and the deposition of α4-laminin. (L) Enlarged cross-sectional view of the engineered vessel, showing that the endothelial cells established well-demarcated apical-basal polarity in correct orientation.

gel. The network consisted predominantly of individual endothelial cells with intercellular connections, which in turn formed continuous lumens, indicative of active vasculogenesis within the 3D matrix system. The lumenal spaces within this capillary network were formed largely through intracellular vacuole formation (Fig. 1D) and coalescence (Fig. 1E). Numerous reports have implicated the formation of intracellular vacuoles, through pinocytosis, as a mechanism for lumen formation in vitro and in vivo during capillary maturation (Davis and Bayless, 2003; Dyson et al., 1976; Folkman and Haudenschild, 1980; Kamei et al., 2006; Montesano and Orci, 1988; Montesano et al., 1987; Nicosia et al., 1982; Wolff and Bar, 1972). Mature vascular networks with prominent lumen formed approximately 3 days after gel assembly (Fig. 1F). The lumenal spaces were further confirmed by transmission electron microscopy (Fig. 1G,H) to be free of extracellular matrix components, indicative of bona fide lumen formation. The lumens in the mature vascular network can also span multiple endothelial cells (Fig. 1I,J), as indicated by anti-VE-cadherin immunofluorescence. It is important to point out that a mature vascular network could be generated with endothelial cells expressing the MLCK FRET sensor (Fig. 1F, Fig. 2, see below), indicating that the MLCK FRET biosensor did not interfere with 3D vascular network formation and maturation.

It was crucial to establish that the endothelial cells in our 3D collagen system form apical-basal polarity. We characterized the deposition of α4 laminin, using 2A3 anti-α4-laminin antibody (Gonzalez et al., 2002) in the 3D collagen matrix relative to the vasculature and the lumenal space. Fig. 1K,L shows the deposition of α4 laminin (red) on the basal side of the vessel and not in the lumen. This result indicates that the endothelial cells successfully establish apical-basal polarity in the correct orientation.

Expressing the MLCK FRET sensor in the 3D vascular network

To create a 3D invasion assay with which we could dynamically study tumor-mediated endothelial cell signaling, we expressed in endothelial cells a FRET-based, Ca^{2+}-calmodulin-sensing, MLCK biosensor (Chew et al., 2002). The Ca^{2+}-calmodulin-dependent MLCK is a key regulator of endothelial permeability. MLCK-mediated myosin-II contraction has been shown to facilitate leukocyte diapedesis and edema formation (Garcia et al., 1995; Garcia and Schaphorst, 1995; Goeckeler and Wysolmerski, 1995; Wysolmerski and Lagunoff, 1990; Wysolmerski and Lagunoff, 1991), thus highlighting MLCK as an ideal candidate for this study. We have previously reported the generation of a FRET sensor that can dynamically detect MLCK activation (Chew et al., 2002). We have since exchanged the low efficiency FRET pair of BFP and GFP to a more robust pair of CFP and YFP (see Materials and Methods). To confirm the occurrence of FRET, acceptor photobleaching was performed in BAPTA-AM-treated endothelial cells expressing the MLCK FRET sensor. The emission spectra demonstrated that the desensitization of YFP was accompanied by a simultaneous recovery in CFP emission intensity (data not shown), confirming the occurrence of FRET, with an average efficiency of 27.6%, calculated from 10 individual cells (data not shown).

We constructed an adenovirus vector expressing the MLCK FRET sensor, allowing us to routinely achieve >90% transfection efficiency for the endothelial cells. As shown in Fig. 1F, overexpression of the biosensor did not interfere with the formation of lumenized 3D vascular network. This is also consistent with previous finding that adenovirus infection did not perturb the ability of endothelial cells to undergo outgrowth, sprouting and anastomosis (Nakatsu et al., 2003).

Breast cancer cells undergo transcellular invasion

To examine how breast cancer cells invade our 3D vascular network, serum-starved MDA MB-231 metastatic breast cancer cells were introduced into the gel either by co-assembly or multi-spot injection via Hamilton syringes. We could observe cells invading the vascular network when the two types of cells came

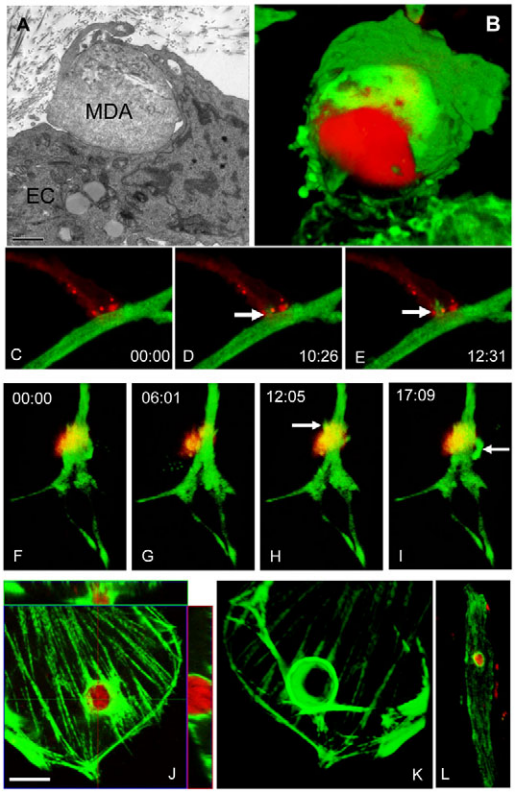

Fig. 2. Dynamic 3D interaction of MDA-MB231 breast cancer cells with the vascular network in vitro. (**A**) Electron micrograph demonstrating the deformation of endothelial cytoplasmic by an MDA-MB231 cell. Note that the tumor cell entered an area next to the endothelial cell nucleus that is devoid of endothelial cell-cell junction. Scale bar: 1 µm. (**B**) 3D reconstruction of confocal microscopy showing the engulfment of an MDA-MB231 cell (red) by an endothelial cell (green). (**C-E**) Time-lapsed confocal microscopy showing the extension of a finger-like protrusion (white arrows) from the endothelial cell (green) towards the MDA-MB231 cell. (**F-I**) Time-lapsed confocal microscopy shows that prolonged interaction with the tumor cell (red) usually triggers active endothelial membrane protrusion and ruffling (arrows). In this case, the endothelial cell protrusive spikes coalesced into a cup-like, actively ruffling structure (see supplementary material Movie 1). The indicated time points are in minutes:seconds. (**J**) Confocal micrographs showing the maximal projection and orthogonal view of the endothelial myosin network in 2D monolayer forming an invasion ring-like structure, encapsulating the invading tumor cell. Scale bar: 5 µm. (**K**) 3D reconstruction of the same invasion ring (180 degree rotation of view from that presented in J) showing a perfectly formed pore through which the tumor cell could gain access to the other side of the endothelium. The cancer cell (red channel) is digitally removed to show the invasion pore. (**L**) Single confocal optical plane across an endothelial cell expressing GFP-RLC within a 3D vessel, indicating that the invasion pores can also form in a 3D vasculature network, in this case surrounding an mCherry-expressing MDA-MB231.

into contact. Tumor cells frequently invaded into individual endothelial cells, and deformed the endothelial cytoplasm in doing so (Fig. 2A). In fact, cancer cells were often seen nearly or completely engulfed inside the capillary lumen (Fig. 2B). Not all interactions resulted in tumor cells initiating and completing a fruitful invasion. Tumor cells also commonly adhered to endothelial cells. This prolonged interaction often triggered active endothelial membrane dynamics; we frequently observed endothelial cells extending finger-like protrusions towards the breast cancer cells (Fig. 2C-E). These protrusions were transient and often underwent several rounds of extension and retraction. In some cases, protrusions coalesced, resulting in highly active membrane ruffles and subsequently forming cup-like structures that would eventually engulf the MDA-MB231 cells. Fig. 2F-I provides a time-lapse 3D documentation of this event (see also supplementary material Movie 1). These rapid cytoskeletal and membranous reorganizations supported our hypothesis that endothelial cells might be involved in initiating and aiding the process of tumor intravasation. Using GFP-tagged myosin-II RLC, we showed that an invading tumor cell is encapsulated by a cytoskeletal network within a single endothelial cell (Fig. 2J). The myosin network formed a pore-like structure that allowed the tumor cell to penetrate through the endothelial cell (Fig. 2K, supplementary material Movie 2), providing strong evidence of transcellular invasion. This invasion pore can also be found in the 3D vessel under tumor invasion (Fig. 2L).

Breast cancer cells transiently activate endothelial MLCK at tumor invasion sites

To test the involvement of endothelial MLCK in tumor invasion, we utilized the high spatio-temporal resolution of our assay to monitor the interaction between tumor and endothelial cells. Fig. 3A (top panels) shows the real-time endothelial MLCK activity during invasion by two MDA MB231 breast cancer cells. The bottom panels of Fig. 3A show the same set of 3D micrographs, but with the cancer cells (red channel) digitally removed to facilitate unobstructed viewing of the ratiometric representation of MLCK activity. The invading tumor cells triggered endothelial MLCK activation. First, there is an elevation of general MLCK activity above baseline on contact with the invading tumor cells, as shown by the drop in the FRET ratio. More importantly, persistent invasion by MDA MB-231 cells triggered a regional and marked decrease of FRET, indicating the activation of MLCK (see supplementary material Movie 3). To highlight the MLCK activation, we plotted the emission intensity profiles of both CFP and YFP as a function of time along the white dotted line (Fig. 3B), spanning both entry sites of the tumor cells. The line scan was performed over the central plane within the 3D vascular volume. As evident from the data, there was a marked increase in CFP emission at the sites of invasion with a concomitant drop of YFP emission. This was a hallmark of FRET loss, indicative of MLCK activation. The endothelial MLCK FRET profile did not change when there was no interaction with tumor cells (supplementary material Fig. S2).

In order to obtain a quantitative analysis of the invasion-mediated endothelial MLCK activity, we compared the FRET ratiometric values in blood vessels invaded by MDA-MB231 cells. Two regions as defined in Fig. 3C were examined. This analysis allowed us to ascertain the relative MLCK activities within the invasion sites as compared with regions of the vasculature distal to the tumor entry site. Our data indicated that endothelial cell MLCK was activated on interaction with tumor cells, with the most pronounced MLCK activity (FRET loss) at the site of endothelial-tumor contact site. In blood vessels not invaded by tumor cells, FRET ratiometric signals remained high, indicating the absence of MLCK activation. This observation demonstrated that invading tumor cells could locally affect the endothelial MLCK activity.

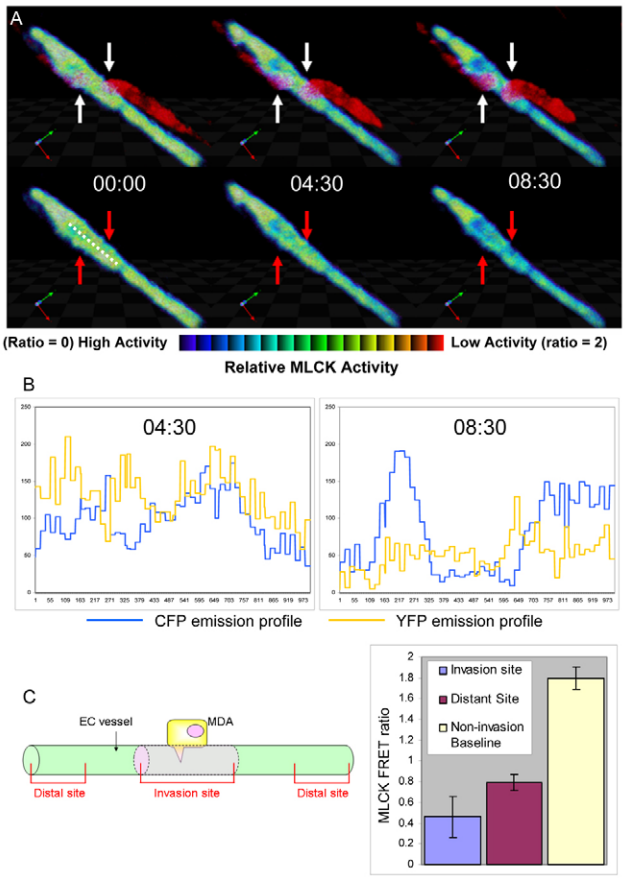

Fig. 3. Breast cancer cells invade the vasculature and induce endothelial MLCK activation. Endothelial cells expressing the MLCK sensor were used to generate a vascular system capable of MLCK signaling read-out during tumor invasion. (**A**) Portion of the blood vessel being simultaneously invaded by two MDA-MB231 breast cancer cells (red cells, white arrows). Relative MLCK activity is displayed using ratio imaging as previously described (Chew et al., 2002). Loss of FRET during MLCK activation turns the ratio color 'bluer', as indicated by the ratio bar. The bottom panels show the identical 3D FRET ratiometric images, but with the red channel, which represents the cancer cells, digitally removed to highlight the FRET changes in the endothelial cell underneath. (**B**) Analysis of the CFP and YFP emission spectra along the indicated dotted line. The invasion of the tumor cells into the endothelium triggered a highly localized drop in YFP emission with a concomitant increase in CFP emission intensity, indicating that MLCK was activated. Indicated time points are in minutes:seconds (n=12) (see supplementary material Movie 2). (**C**) Left: Pre-defined regions for quantitative analysis of invasion-mediated MLCK activation. The 'invasion site' is defined as the region centered on the tumor entry site, spanning the length of three tumor cells. A 'distal site' is defined as the region of the same vessel tube at least two cell-lengths away from the invading cancer cell. Right: 21 invasion events were analyzed and the average FRET ratio changes were plotted. Lower FRET ratio corresponds to higher MLCK activity. Vessels that are not in contact with tumor cells serve as FRET ratio baseline. Error bars represent s.e.m.

Interaction with tumor cells triggers elevation of Ca^{2+} levels in endothelial cells

The FRET sensor reports MLCK activity by way of MLCK colocalization with Ca^{2+}-calmodulin. For the endothelial MLCK to be modulated by invading breast cancer cells, the endogenous Ca^{2+} level within the endothelial cell must likewise be affected. This provided an excellent basis for a stringent test using the Cameleon calcium sensor (Miyawaki et al., 1997) to reciprocally confirm our observation with the MLCK FRET sensor. Whereas our sensor detects the Ca^{2+}-calmodulin complex through the loss of FRET, the Cameleon sensor detects Ca^{2+} levels through the gain of FRET. We opted for the Cameleon sensor, rather than commercially available Ca^{2+} dyes, as a means to keep the working conditions constant with respect to the imaging technique (FRET) and the donor-acceptor pair (CFP-YFP). Endothelial cells expressing the Cameleon sensor were used to build a similar 3D vasculature system, and MDA MB-231 cancer cells were allowed to invade the engineered vasculature.

As shown in Fig. 4, the interaction with tumor cell induced a rapid increase in endogenous Ca^{2+} level within the endothelial cell. Note that the increase in free Ca^{2+} within the endothelial cells revealed a slightly different pattern than that detected by the MLCK FRET sensor. The Cameleon sensor showed a more general elevation of free Ca^{2+} throughout the endothelial cells, whereas the MLCK FRET sensor indicated MLCK binding to Ca^{2+}-calmodulin mainly at the site of active contraction, consistent with previous findings that MLCK activation is localized (Chew et al., 2002). It was not surprising that there was no complete overlap of elevation patterns between free Ca^{2+} and the complex of MLCK-Ca^{2+}-calmodulin. However, the findings from both sensors were consistent: interaction with tumor cells increased Ca^{2+}-mediated signals within the underlying endothelial cells.

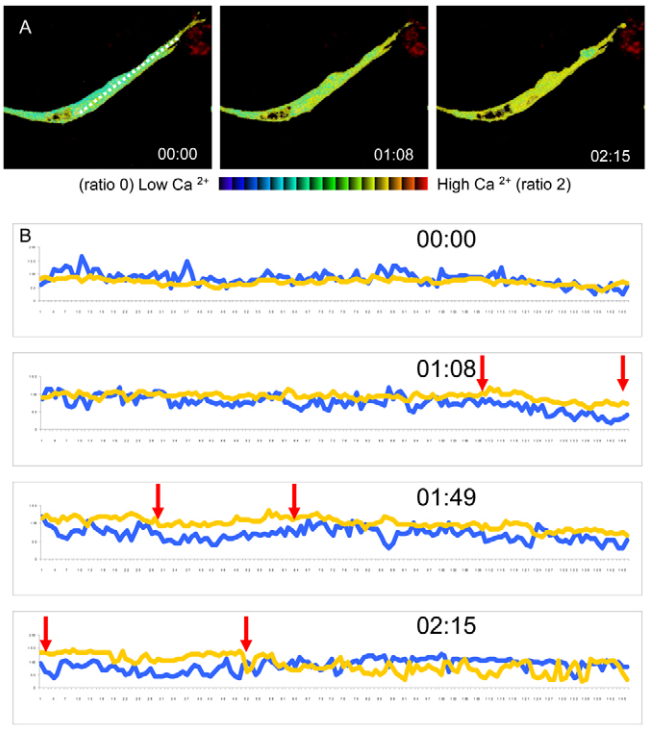

Fig. 4. Cameleon biosensor indicates an increase in intracellular Ca^{2+} in endothelial cells. (**A**) Time-lapse 3D FRET ratiometric confocal micrographs of Cameleon sensor in an endothelial cell. The interaction with a MDA-MB231 cell (red) induced a Ca^{2+} wave that was rapidly propagated along the entire length of the endothelial cell. The Ca^{2+} wave is ~30% above baseline. (*n*=3 out of 3) All indicated time points are in minutes:seconds. (**B**) Real-time raw intensity profiles of CFP and YFP from the Cameleon sensor along the white dotted line over the endothelial cell in Fig. 4A. Red arrows bracket the regions with increase FRET activity (high Ca^{2+} concentration). Note the propagation of the Ca^{2+} front from the initial tumor interaction site.

Phosphorylated myosin-II RLC is enriched locally at the site of MDA-MB231 transcellular invasion

MLCK is a highly specific kinase with only one known physiological substrate (Bresnick, 1999; Kamm and Stull, 2001): the 20 kDa RLC that regulates the actin-activated ATPase of myosin-II. Unlike Rho kinase (ROCK), which mono-phosphorylates RLC at residue Ser19 (Amano et al., 1996), MLCK is capable of diphosphorylating RLC at Ser19 and Thr18 (Stull et al., 1990). Phosphorylation of the RLC at Ser19 potentiates myosin ATPase 10- to 100-fold (Stull et al., 1990), whereas diphosphorylation of RLC at Ser19 and Thr18 maximally activates

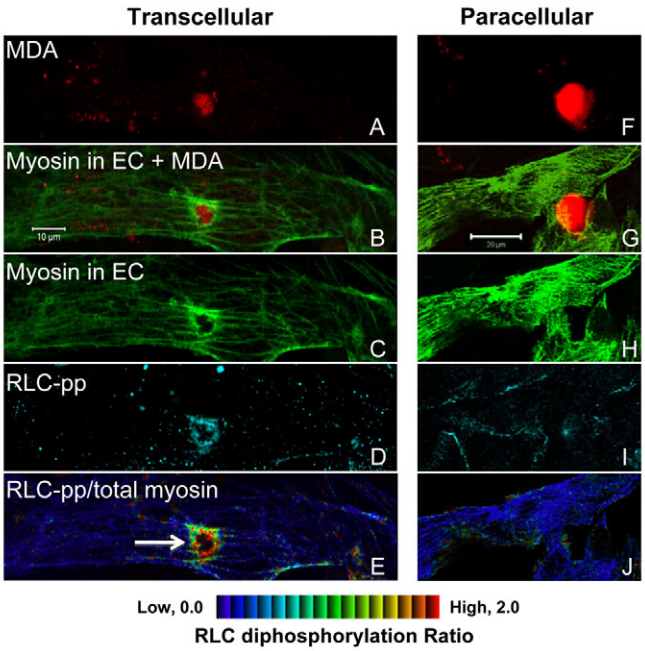

Fig. 5. Enrichment of diphosphorylated RLC at transcellular invasion site in endothelial cells. (**A**) MDA-MB231 cell transiently expressing untagged mCherry fluorescent protein. (**B**) Overlay of endothelial myosin network (green) and an MDA-MB231 cell undergoing transcellular migration. Note the myosin ring that surrounds the tumor cell. Scale bar: 10 µm. (**C**) Endothelial myosin network as displayed by GFP-RLC. (**D**) Immunofluorescence with antibody specific for the diphosphorylated (phosphorylated at Thr18 and Ser19) form of RLC (RLC-pp). (**E**) The distribution of diphosphorylated RLC was assessed by determining the ratio of phosphorylated RLC (from D) to total myosin-II (from C), and displayed according to the ratio bar. Myosin with very high phosphorylated RLC is indicated in red (white arrow). 26 out of 27 transcellular invasion events showed marked increase in RLC diphosphorylation around the invasion ring. (**F-J**) Comparable analyses were performed on MDA-MB231 cells undergoing paracellular invasion. A representative invasion event is presented here. Scale bar: 20 µm. None of the 31 paracellular invasion events analyzed displayed myosin ring formation. A representative paracellular invasion event is shown. These assays were performed on a 2D surface to allow for accurate ratiometric imaging analysis.

myosin-II. The marked in situ activation of MLCK suggests that the endothelial myosin-II RLC might be locally targeted for maximal phosphorylation. To test this hypothesis, we performed immunofluorescence using antibodies specific for the diphosphorylated form of RLC (Fig. 5D). GFP-tagged RLC served as baseline control for myosin-II local concentration, irrespective of phosphorylation state (Fig. 5C). MDA-MB 231 tumor cells were transiently transfected with untagged mCherry protein to serve as volume marker (Fig. 5A). The relative level of RLC phosphorylation was obtained by normalizing the level of phosphorylated RLC to total myosin-II local concentration as previously described (Chew et al., 2002). As shown (Fig. 5E), diphosphorylated RLC is enriched in the endothelial myosin structure that encapsulates the invading tumor cell.

In paracellular invasion events (Fig. 5F-J), neither of the adjacent endothelial cells that border the invading tumor form a ring-like myosin structure. Small clusters of diphoshorylated RLC can be observed around the invasion site (Fig. 5J), as well as cortical actin structures. The level of diphosphorylated RLC concentration, however, is significantly lower than that found in the transcellular invasion ring.

MLCK activation mediates localized endothelial myosin-II contraction at the tumor entry site

Our data suggest that invasive tumor cells might locally activate endothelial myosin. To test this hypothesis, individual stress fiber lengths within the endothelial cell were measured during tumor invasion. Only stress fibers with both ends clearly discernible in 3D throughout the course of invasion were taken into consideration. As shown in Fig. 6A, active shortening of endothelial cell stress fibers occurred locally at the site of invasion. This localized stress fiber contraction was consistent with MLCK activation, and suggested an active role of endothelial cells in mediating tumor transcellular intravasation.

In order to accurately quantify the rate of myosin contractile activity, measurement of myosin-II sarcomeric distance was performed (Fig. 6B). The lack of imaging resolution in thick collagen gel precluded the possibility of performing this experiment in 3D. We allowed tumor cells to invade into a 2D monolayer of endothelial cells expressing GFP-tagged RLC, and the rate of myosin contraction was measured as described (Fig. 6B,C). Consistent with our RLC phosphorylation ratiometric studies (Fig. 5), myosin contractile activity was markedly potentiated around the

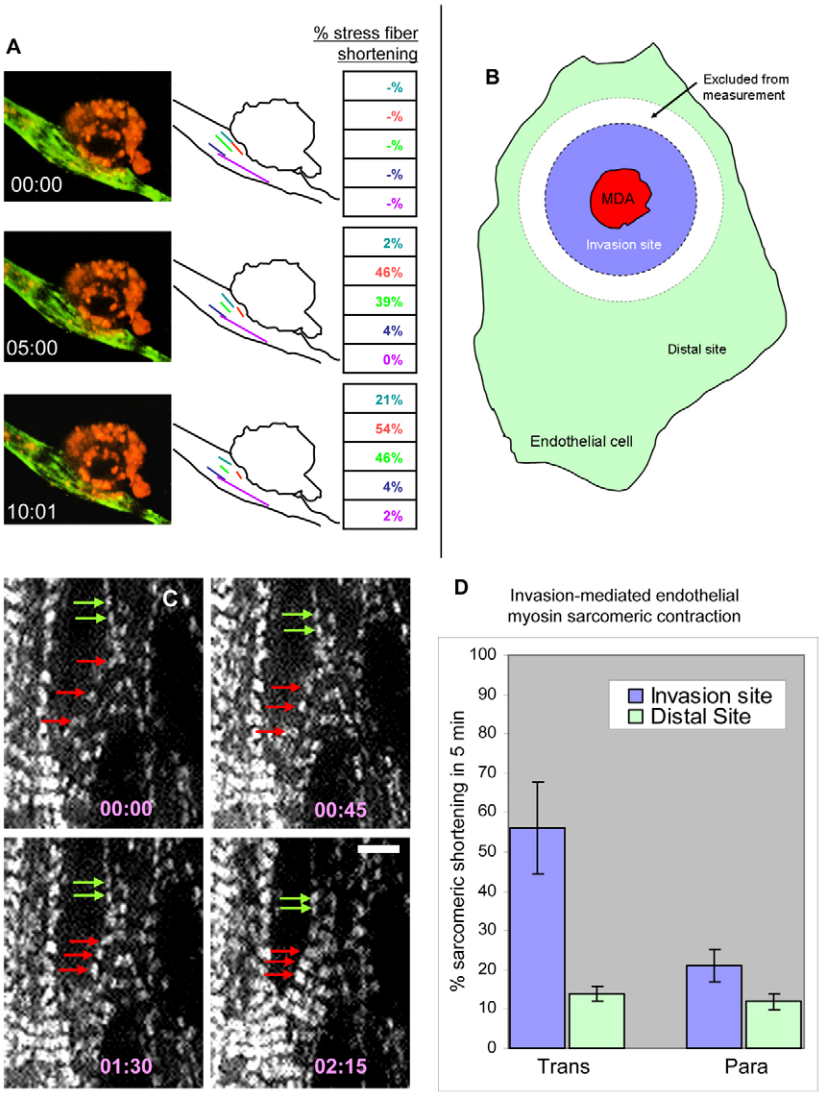

Fig. 6. Elevation of endothelial myosin-II contractile activity at transcellular invasion site. (**A**) Confocal micrograph of MDA-MB231 (red) transcellular invasion into an endothelial cell expressing GFP-RLC. (middle panels) Outline of the cells and five prominent endothelial stress fibers are presented. (right panels) Myosin-II contraction is expressed as a percentage stress-fiber shortening as compared with the initial lengths. The color of the % matches the color of the stress fiber outline (four of four invasion events showed regional stress-fiber shortening. Representative cell is shown). Indicated time points are in minutes:seconds. (**B**) To obtain a quantitative analysis of local increased rate of myosin contraction, two distinct regions were pre-defined. The 'invasion site' (blue) is defined as the region centered on the tumor entry site, spanning the diameter of three tumor cells. A 'distal site' (green) is defined as the region of the same vessel tube at least two cell-diameters away from the invading cancer cell. To eliminate potential overlap, we avoided the region immediately surrounding the invasion site (white). (**C**) High resolution time-lapse 2D spinning disk confocal micrographs showing how sarcomeric distance as indicated by GFP-RLC can be measured. Time is in minutes:seconds. Scale bar: 2 μm. Red and green arrows denotes two separate sets of sarcomeres being measured. The actual invasion ring usually contains myosin sarcomeres too compact to be included for accurate measurement. (**D**) Rate of myosin contraction as determined by the shortening of inter-sarcomeric distance (% shortening in 5 minutes) during transcellular and paracellular invasion. Results from eight transcellular (Trans) and eight paracellular (Para) events are plotted (total number of sarcomeres measured was 126). Error bars represent s.e.m.

transcellular invasion ring and, to a much lesser extent, in paracellular invasion sites (Fig. 6D).

RLC phosphorylation affects the tumor invasion route

Data presented thus far demonstrate that tumor cells undergoing transcellular invasion cause activation of MLCK-mediated endothelial myosin. To test the role of RLC phosphorylation in determining the intravasation route, we overexpressed GFP-tagged non-phosphorylatable RLC (Ala substitution of Thr18 and Ser19, hereafter referred to as 18A19A RLC) mutant in endothelial cells. The expression of 18A19A mutant did not affect the integrity of the endothelial cell borders (supplementary material Fig. S3). In order to obtain a high number of tumor invasion events for statistical analyses, we adapted the assay previously used for studying leukocyte transendothelial diapedesis (Carman and Springer, 2004). Taking advantage of the powerful tissue cytometry capability of the TissueGnostics system, we devised an unbiased, sequential gating strategy to rapidly screen large population of cells (described in Materials and Methods). This technique allowed us to score a large number of invasion events for comparing transcellular and paracellular routes.

MDA MB-231 cells underwent paracellular (44%) and transcellular (56%) invasion through endothelial cells expressing wild-type RLC (Fig. 7). However, when challenged with endothelial cells overexpressing 18A19A RLC, tumor cells overwhelmingly bypassed transcellular invasion (21%) and transmigrated via the paracellular route (79%). This result implicated the direct involvement of endothelial contractile function in mediating the tumor intravasation.

Discussion

Engineering a lumenized 3D vascular network with dynamic FRET read-out capability

The interaction between tumor and endothelial cells during intravasation has hitherto been poorly characterized for several reasons. First, transendothelial migration is transient and localized, posing a huge challenge to any effort to study this momentary occurrence. In addition, both cancer and endothelial cells can elicit distinct response when cultured in a 3D environment in which tension distribution is drastically different from that on 2D culture dishes (Bell et al., 2001; Darland and D'Amore, 2001; Davis et al., 2007; Mierke et al., 2008a). Second, assays that employ conventional 2D culture conditions, although instrumental in identifying molecular components and signaling pathways, do not provide accurate assessment of force generation during invasion that takes place physiologically within dense connection tissue. Third, most assays are directed towards the invasive potential of the cancer cells, and consider the underlying endothelium as a passive and permissive component in the process. Taken together, these problems underscore the need to alter our way of studying signal transduction during tumor intravasation. We have devised a culture system wherein endothelial cells form a 3D vascular network. We then integrated the resolving power of FRET into this 3D system to dissect the MLCK activity during tumor invasion.

Invasive mechanism of breast cancer cells in 3D milieu

The endothelial cells in our assay system did not attract the cancer cells, and the MDA MB-231 cells did not undergo directed chemotaxis toward the vasculature (data not shown). This observation by no means argues against reports that implicate cancer cell chemotaxis towards the blood vessel in vivo (Kedrin et al., 2008). Instead, our observation is fully anticipated, as there is no blood flow in the in vitro vascular network. The cancer cells are not migrating directionally towards the source of any hematogenous growth factor. However, upon random cell-cell interaction, MDA-MB231 cells would invade into the 3D vascular network. We routinely observed the cancer cells undergoing intravasation through both transcellular and paracellular routes. Transcellular migration is a common mechanism in leukocyte diapedesis (Carman and Springer, 2004; Millan et al., 2006; Nieminen et al., 2006), highlighting the intrinsic ability of endothelial cells to facilitate this mode of entry. This notion is supported by the finding that the rate of leukocyte transcellular diapedesis is dependent on the lineage of the underlying endothelial cells (Carman and Springer, 2004), implicating intra-endothelial signals in determination of the route of intravasation. Data presented here provide evidence that the invading tumor cells can also be involved in intra-endothelial signaling in order to provide a mechanism for entry into the bloodstream.

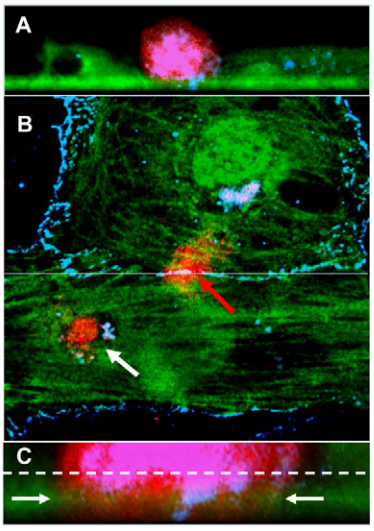

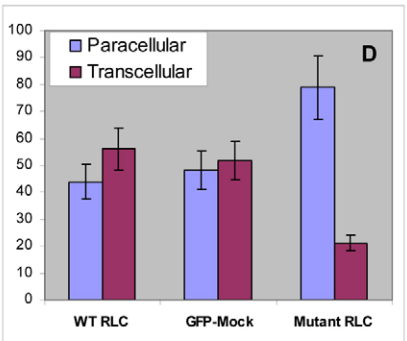

	WT RLC		GFP-Mock		Mutant RLC	
	Cell Count	%	Cell Count	%	Cell Count	%
Paracellular	62	43.97	55	48.25	67	78.82
Transcellular	79	56.03	59	51.75	18	21.18

Fig. 7. MDA-MB231 transcellular invasion is dependent on phosphorylation of endothelial myosin-II RLC. (**A**) Orthogonal view of confocal micrograph showing example of a paracellular invasion event; MDA-MB 231 cell (red), VE-cadherin (light blue), GFP-RLC (green). (**B**) Confocal micrograph showing example of how paracellular (red arrow) and transcellular (white arrow) invasions are scored. Grey horizontal line indicates the cross-sectional cut of which the orthogonal view is presented in C. (**C**) Magnified orthogonal view showing the location of VE-cadherin along the Z-axis, which is found near the bottom slice of the Z-stacks (<900nm from the coverslip). Arrows show that at this Z location, the breast cancer cell would have penetrated the endothelial layer. Only images from this Z-section were used for image analysis. (**D**) Bar graphs and table showing the actual cell count and the percentage of MDA-MB231 invasion via paracellular and transcellular routes when challenged by endothelial cells expressing wild-type or mutant RLC. Endothelial cells mock-transfected with empty pEGFP-C1 vector serve as control.

Invading tumors trigger activation of MLCK-mediated endothelial myosin-II at the entry sites

We demonstrated that the MLCK-mediated myosin-II contractile function is a component of intra-endothelial signals during tumor invasion. The transient elevation of MLCK activity is mediated by Ca^{2+}-calmodulin, as reciprocally confirmed by two separate FRET sensors. This Ca^{2+}-dependent event correlates well with the formation of transcellular pores in endothelial cells during leukocyte diapedesis, which can also be abrogated by Ca^{2+} chelation (Carman and Springer, 2004). Taken together, these findings implicate a synergistic signal that might simultaneously mediate multiple mechanisms in transcellular invasion.

We confirmed that RLC phosphorylation increased in correlation with MLCK activity at the invasion site. Our immunofluorescence experiments were performed with antibody specific for Ser19 and Thr18 diphosphorylated RLC, and not Ser19 monophosphorylated RLC. Therefore, the increase of RLC phosphorylation reported in our ratiometric study was due to MLCK activation. We cannot rule out the signals of Rho family GTPases in this assay, such as ROCK (Amano et al., 1996) or p21-activated kinases (Chew et al., 1998; Zeng et al., 2000), which monophosphorylate RLC at Ser19. Even though these signaling pathways converge on RLC, they modulate distinct myosin functions. ROCK activity contributes to the integrity of stress fibers in anchored cells (Amano et al., 1997; Totsukawa et al., 2000) and tail retraction in motile cells (Worthylake et al., 2001). Conversely, MLCK can swiftly and maximally potentiate myosin-II activity due to its high V_{max} and cause rapid shortening of stress fibers. We have previously shown that MLCK can be rapidly sequestered along actively shortening stress fibers (Chew et al., 2002), suggesting that it might work optimally at high local concentration.

We argued against the use of inhibitors such as Y27632 or ML-7 to dissect these signals. Drug treatment would affect both cell types in this co-culture system and preclude accurate data interpretation. Instead, challenging the tumor cells with endothelial cells expressing non-phosphorylatable RLC provides a cleaner assessment, and our results confirm that tumor transcellular invasion is dependent on endothelial RLC diphosphorylation.

Signaling events during transcellular invasion

The role of RLC phosphorylation in leukocyte migration across the endothelium has been strongly supported by evidence that calyculin treatment of endothelial cells led to accumulation of phosphorylated RLC and significantly enhanced diapedesis (Verin et al., 1995). In fact, adherent neutrophils have been shown to directly activate endothelial MLCK in situ (Garcia et al., 1998; Hixenbaugh et al., 1997). Hence, the interaction with tumor cells might directly modulate endothelial cell cytoskeletal function, and subsequently transendothelial migration.

It is unclear how tumor cells elevate endothelial Ca^{2+} levels, but the process is probably mediated by cell-surface receptors. Tumor-related adhesion molecules such as CD24 and $\alpha4\beta1$ integrin are known to bind to endothelial P-selectin and VCAM-1. Both P-selectin and VCAM-1 can induce an increase in endothelial Ca^{2+} when engaged and lead to cytoskeletal rearrangement (Lorenzon et al., 1998), highlighting these molecules as prime candidates for further studies.

The role of myosin-II contraction in transcellular invasion

Studies on immunologic transcellular migration offer an important framework with which we can consider the role of the endothelial contractility in tumor intravasation. The intermediate filament (IF) network is required in both the opposing endothelial cells and in the migrating peripheral blood mononuclear cells to form an anchoring structure that stabilizes the interaction (Nieminen et al., 2006). IF networks of both endothelial cells and lymphocytes undergo reorganization, and form a cage around the migrating cells prior to transcellular diapedesis. IF is highly resistant to mechanical stress and has been proposed to play a crucial role in the conveyance of cytoskeletal crosstalk (Coulombe and Wong, 2004). The actin filaments, microtubules and IF networks are inextricably interconnected by molecular crosslinkers such as plectin (Wiche, 1998). Therefore, the formation of an IF cage around the migrating cells might provide a molecular handle with which the endothelial contractile machinery can pull the incoming cell into the lumen (Fig. 8). Likewise, our data show that the endothelial myosin network can indeed form a pore structure around the invading tumor cell, and that myosin activity is potentiated at the invasion site for rapid contraction. It is thus consistent with our observation that abrogating the endothelial contraction severely curtailed the tumor transcellular migration. Another aspect that should be considered is that myosin contraction could provide mechanical resilience to restrict the size of the invasion pore and prevent the endothelial cells from being ripped apart.

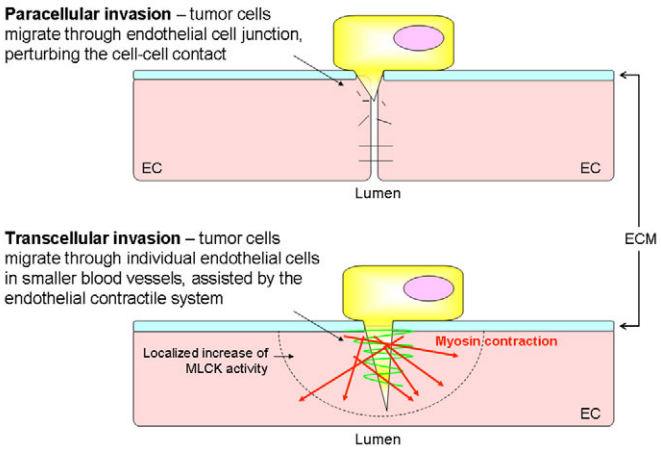

Fig. 8. Postulated role of myosin-II contraction in tumor intravasation. Schematic illustration of how myosin-II could contribute to the paracellular and transcellular routes of tumor intravasation. Top: in the paracellular route, perturbation of endothelial junctional complexes allows tumor cells to undergo paracellular intravasation. Myosin-II contraction will probably increase gap size and facilitate tumor cell transmigration. However, the disruption of endothelial cell-cell junctions might be sufficient to allow the passage of highly invasive tumors. Bottom: in the transcellular invasion model, the endothelial intermediate filaments (green lines) might form a highly interconnected cytoskeletal cage around the invading tumor cell, in close resemblance to leukocyte trafficking (Nieminen et al., 2006). The highly crosslinked cytoskeletal network provides a molecular handle with which the active endothelial myosin-II contraction can facilitate the entrance of a tumor cell into the endothelial lumen.

Conclusion

This study provides new insight into how the endothelial signaling cascades might be modulated by the invading tumor, and highlights the importance of examining the process of tumor invasion from an important yet hitherto under-explored perspective – that of the underlying endothelium. The dependence of tumor invasion route on endothelial contractility provides an important reminder that

tumor intravasation is a host-disease interaction, and that the endothelium might serve as key determinant in tumor invasive potential. Successful tumor invasion is the sum result of many factors that constitute the tumor microenvironment (Condeelis and Pollard, 2006; Kedrin et al., 2008; Li et al., 2007; Lunt et al., 2008; Witz, 2006; Witz, 2008), which is experimentally difficult to scrutinize. Our system offers a powerful way to reconstitute the cellular, chemical and physical environment, one element at a time if necessary, to dissect the tumor invasion mechanisms. Our immediate future goal is to engineer a similar 3D vessel using lymphatic endothelial cells, as the lymphatic system represents the common route through which many cancers metastasize. However, the engineered vascular network as a tumor invasion platform underscores our ability to control the genotype of the cellular players in the tumor microenvironment at will, allowing us to introduce cell-type-specific gene manipulation without having to resort to drug treatment, which invariably affects all cells in the tumor milieu.

Materials and Methods

Constructs

The construction of the MLCK FRET biosensor was described previously (Chew et al., 2002). We have modified this biosensor for the present study by replacing the donor-acceptor pair of BFP-GFP with CFP-YFP. Both the CFP and YFP cDNAs were PCR-amplified from the appropriate vectors of the 'Living Colors' vector series purchased from Clontech Laboratories. The MLCK FRET sensor construct was inserted into the Gateway pENTR-3C vector (Invitrogen) by directional cloning at the *Kpn*I and *Not*I sites, and recombined with pAd/CMV/V5-DEST expression vector according to the Invitrogen Gateway LR recombination protocol. The adenovirus was produced in HEK293A cells, and titered using the manufacturer's protocol.

Cell culture and transfection

Calf pulmonary artery endothelial cells (ATCC) were cultured in DMEM (Invitrogen-Gibco) supplemented with 20% fetal calf serum (Hyclone), 1 mM sodium pyruvate, 1 mM glutamine, MEM non-essential amino acids, and penicillin-streptomycin, buffered in 5% CO_2 and incubated at 37°C. MDA MB-231 breast cancer cells (ATCC) were cultured in Leibovitz-15, or L-15 medium (Invitrogen-Gibco) supplemented with 10% fetal calf serum (Hyclone), 1 mM sodium pyruvate and penicillin-streptomycin. The cancer cells were grown in a 37°C incubator without CO_2.

Engineering 3D vasculature in vitro

3D gels were assembled in 50 mm 'FluoroDish' with coverslip bottom from World Precision Instruments (www.wplinc.com) as shown in supplementary material Fig. S1A. The porous ring was cut from a long one-quarter inch polypropylene tube (www.smallparts.com), and secured onto the dish with autoclaved vacuum grease. Endothelial cell suspension was then mixed with 0.5 ml 2× concentration collagen gel master mix, to be co-assembled into 1 ml final volume of cell-collagen mixture. At final concentration (1×), the collagen gel mix consisted of 1.2 mg/ml type I collagen, 0.6 mg/ml Matrigel (BD Sciences), 1× Hank's balanced salt solution (Cellgro), 3 μg/ml laminin-10, buffered by 0.04% sodium bicarbonate. The pH of the gel was adjusted to 7.4 with sodium hydroxide before cells were added. The cell-collagen mixture was allowed to solidify for 15 minutes at room temperature. 1.5 ml EGM-2MV medium (supplied as a kit by Lonza) was then added before returning the dish to the incubator. MDA-MB231 cells were introduced into the gel by either co-culturing or by multi-spot injection through a Hamilton syringe.

Live cell imaging

Live cell imaging was performed on Zeiss LSM510 META laser scanning confocal microscope or Olympus DSU spinning disc confocal as indicated. The occurrence of FRET within the biosensor was confirmed by acceptor photobleaching in endothelial cells treated with BAPTA-AM to chelate intracellular calcium in order to maximize FRET. The photobleaching of YFP results in a concomitant increase in CFP emission intensity in the event that FRET occurs. FRET efficiency (E_{FRET}) was calculated using the formula $E_{FRET}=(I'-I) \times 100/I'$ where I and I′ are the CFP fluorescence intensities before and after YFP photobleaching, respectively.

Dynamic 3D live cell FRET imaging was performed mainly on an Olympus DSU spinning disk confocal microscope equipped with I×81 zero-drift compensation (ZDC) device for active focal plane maintenance. The 3D matrix was kept in EGM-2MV medium at 37°C and 5% CO_2 by means of a Tokai Hit on-stage incubation chamber. Automated image acquisition was driven by Slidebook software v4.2 (Intelligent Imaging Innovations, Santa Monica, CA). Time-lapse optical sectioning was performed at 120-160 milliseconds exposure with a ~50 millisecond interval between images without saturated pixels. To avoid any potential motion artifact, the software was programmed to alternate the image acquisition sequence (i.e. AB, BA, AB… instead of AB, AB, AB…). In order to correct for potential fluorescent bleed-through, images were initially acquired as described by the Youvan method (Youvan et al., 1997) to correct for fluorescent crosstalk.

Ratiometric 3D FRET image display and analysis

MLCK activity was displayed as previously described (Chew et al., 2002). This method has the advantage of displaying not only the relative MLCK activity, but also the relative level of protein concentration. Briefly, the ratio comprises of the numerator F_{FRET} (YFP emission, with CFP excited) and the denominator F_{YFP} (YFP emission, with YFP excited). 3D ratio images were constructed using Volocity 5.0 software (Improvision) through intensity-modulated display, in which the ratio is displayed in 16 different color hues with the lowest ratio (MLCK active) displayed at the blue end of the ratio spectrum. Using the intensity of the denominator (which serves as the internal control of MLCK relative concentration, irrespective of FRET), the ratio colors were displayed in 16 different intensity levels by the intensity-modulated display (as shown in Fig. 3), allowing us to combine the simultaneous display of MLCK activation and protein concentration profiles. To dissect the FRET signal within the underlying endothelium during tumor invasion (Figs 3 and 4), a line scan was performed across the central optical plane of the vessel for both the CFP and the YFP channels. To reciprocally confirm the Ca^{2+}-based signal triggered by tumor cells, we utilized the Cameleon Ca^{2+} FRET sensor. The expression of the sensor in mammalian cells was driven by the BacMam baculovirus delivery system (Invitrogen). Endothelial cells were infected by the viral stock according to the manufacturer's protocol, and assembled into the 3D collagen gel as described in the previous section. FRET ratiometric imaging was then performed in an identical fashion to that described for the MLCK sensor. In the case of Cameleon, a gain in FRET signifies an increase in Ca^{2+} levels.

Quantification of shortening of endothelial cell stress fibers in 3D gel

Stress fibers in endothelial cells were visualized using GFP-tagged myosin-II RLC. Both GFP-tagged wild-type and mutant RLC were generous gifts from Rex Chisholm (Northwestern University Feinberg School of Medicine, Chicago, IL). Myosin-II contraction was quantified from the rate of stress fiber shortening within the 3D gel, and was measured using 'Filament Length' module of the Volocity software.

Measurement of myosin contractile activity was performed using Volocity. Regions of interest, as defined in Fig. 6B, were first cropped and imported into Volocity. Thresholding of the monochrome images allowed us to easily identify and digitally mask individual sarcomeric units. The rate of myosin contraction was then measured as defined by the centroid of each sarcomere. Individual measurements were abandoned following the fusion of two or more centroids.

Quantification of transendothelial invasion

Endothelial cells expressing the GFP-tagged wild-type or mutant RLC were plated onto coverslips inside 35-mm tissue culture dishes. At 2 days after cells reached confluency, MDA-MB231 cells labeled with CellTracker Red were plated on top of the confluent endothelial monolayer and allowed to invade into the monolayer for 60 minutes. The dishes were then washed to remove any MDA-MB231 cells that were not attached, and the specimens were fixed. The endothelial cell borders were then stained with anti-VE cadherin antibody and visualized with Alexa-Fluor-633-conjugated secondary antibody.

Confocal sections were obtained with a Zeiss LSM510 (1.0 Airy unit) from random fields on the coverslips in a blinded experiment. Images were imported into TissueQuest tissue cytometric software (TissueGnostics, Vienna, Austria; www.tissuegnostics.com). Individual cells (both endothelial and breast cancer cells) were identified by the software via DAPI staining. The populations of cancer and endothelial cells were then plotted on a scattergram, and could be clearly delineated by their red and green intensities, respectively. The cancer cell population was then gated from the scattergram for further analysis, in an identical fashion to the method used for a flow cytometer (further described in www.tissuegnostics.com). To distinguish between paracellular and transcellular invasion, a second scattergram (red vs. Alexa Fluor 633) was plotted. We further gated the cancer cells into two populations by their colocalization with the Alexa-Fluor-633-stained VE cadherin. Paracellular invasion would dictate the colocalization of the cancer cells with the endothelial VE cadherin border (Fig. 7B). This sequential gating process by the TissueQuest software allowed us to rapidly screen a large population of cells purely by their intensities and colocalization profiles, without being biased by morphology.

Reagents, proteins and antibodies

Type I collagen was prepared as previously described (Choe et al., 2003; Parkhurst and Saltzman, 1992). CellTracker Red and CellTrace Oregon Green were purchased from Invitrogen (Eugene, OR). Goat polyclonal IgG anti-VE cadherin antibody was purchased from Santa Cruz Biotechnology. We obtained the monoclonal anti-myosin-II heavy chain antibody from Covance. Rabbit polyclonal antibody against diphosphorylated (Thr18 and Ser19) RLC was supplied by Cell Signaling Technology (Danvers, MA). Secondary antibodies of Alexa-Fluor-633-conjugated donkey anti-goat and Alexa-Fluor-633-conjugated anti-mouse IgM were purchased from Invitrogen. 2A3 antibody against the G domain of α4 laminin was a generous gift from Jonathan Jones, Northwestern University Feinberg School of Medicine (Gonzalez et al., 2002).

This work was supported by the Department of Defense Breast Cancer Research Program Idea Award W81XWH-06-1-0345 (T.L.C.), VA Merit Review (P.H.S.S.), HL-45788 and P20-RR16440 from the National Institutes of Health (R.B.W.). All microscopy works were performed at Northwestern University Cell Imaging Facility supported in part by P30 CA60553 from the National Cancer Institute (NIH). We thank Rex L. Chisholm for his generous support, as well as Anthony Kowal and Aisha Nair for their help throughout the course of this work. Deposited in PMC for release after 12 months.

Supplementary material available online at
http://jcs.biologists.org/cgi/content/full/123/3/431/DC1

References

Amano, M., Ito, M., Kimura, K., Fukata, Y., Chihara, K., Nakano, T., Matsuura, Y. and Kaibuchi, K. (1996). Phosphorylation and activation of myosin by Rho-associated kinase (Rho-kinase). *J. Biol. Chem.* **271**, 2026-2029.

Amano, M., Chihara, K., Kimura, K., Fukata, Y., Nakamura, N., Matsuura, Y. and Kaibuchi, K. (1997). Formation of actin stress fibers and focal adhesions enhanced by Rho-kinase. *Science* **275**, 1308-1311.

Bell, S. E., Mavila, A., Salazar, R., Bayless, K. J., Kanagala, S., Maxwell, S. A. and Davis, G. E. (2001). Differential gene expression during capillary morphogenesis in 3D collagen matrices: regulated expression of genes involved in basement membrane matrix assembly, cell cycle progression, cellular differentiation and G-protein signaling. *J. Cell Sci.* **114**, 2755-2773.

Bresnick, A. R. (1999). Molecular mechanisms of nonmuscle myosin-II regulation. *Curr. Opin. Cell Biol.* **11**, 26-33.

Carman, C. V. and Springer, T. A. (2004). A transmigratory cup in leukocyte diapedesis both through individual vascular endothelial cells and between them. *J. Cell Biol.* **167**, 377-388.

Chew, T. L., Masaracchia, R. and Wysolmerski, R. (1998). Phosphorylation of non-muscle myosin II regulatory light chain by p21-activated kinase (gamma-PAK). *J. Muscle Res. Cell Motil.* **19**, 839-854.

Chew, T. L., Wolf, W. A., Gallagher, P. J., Matsumura, F. and Chisholm, R. L. (2002). A fluorescent resonant energy transfer-based biosensor reveals transient and regional myosin light chain kinase activation in lamella and cleavage furrows. *J. Cell Biol.* **156**, 543-553.

Choe, M. M., Sporn, P. H. and Swartz, M. A. (2003). An in vitro airway wall model of remodeling. *Am. J. Physiol. Lung Cell Mol. Physiol.* **285**, L427-L433.

Condeelis, J. and Pollard, J. W. (2006). Macrophages: obligate partners for tumor cell migration, invasion, and metastasis. *Cell* **124**, 263-266.

Coulombe, P. A. and Wong, P. (2004). Cytoplasmic intermediate filaments revealed as dynamic and multipurpose scaffolds. *Nat. Cell Biol.* **6**, 699-706.

Darland, D. C. and D'Amore, P. A. (2001). TGF beta is required for the formation of capillary-like structures in three-dimensional cocultures of 10T1/2 and endothelial cells. *Angiogenesis* **4**, 11-20.

Davis, G. E. and Bayless, K. J. (2003). An integrin and Rho GTPase-dependent pinocytic vacuole mechanism controls capillary lumen formation in collagen and fibrin matrices. *Microcirculation* **10**, 27-44.

Davis, G. E., Koh, W. and Stratman, A. N. (2007). Mechanisms controlling human endothelial lumen formation and tube assembly in three-dimensional extracellular matrices. *Birth Defects Res. C. Embryo Today* **81**, 270-285.

Dyson, S. E., Jones, D. G. and Kendrick, W. L. (1976). Some observations on the ultrastructure of developing rat cerebral capillaries. *Cell Tissue Res.* **173**, 529-542.

Folkman, J. and Haudenschild, C. (1980). Angiogenesis in vitro. *Nature* **288**, 551-556.

Garcia, J. G. and Schaphorst, K. L. (1995). Regulation of endothelial cell gap formation and paracellular permeability. *J. Investig. Med.* **43**, 117-126.

Garcia, J. G., Davis, H. W. and Patterson, C. E. (1995). Regulation of endothelial cell gap formation and barrier dysfunction: role of myosin light chain phosphorylation. *J. Cell Physiol.* **163**, 510-522.

Garcia, J. G. N., Verin, A. D., Herenyiova, M. and English, D. (1998). Adherent neutrophils activate endothelial myosin light chain kinase: role in transendothelial migration. *J. Appl. Physiol.* **84**, 1817-1821.

Goeckeler, Z. M. and Wysolmerski, R. B. (1995). Myosin light chain kinase-regulated endothelial cell contraction: the relationship between isometric tension, actin polymerization, and myosin phosphorylation. *J. Cell Biol.* **130**, 613-627.

Gonzalez, A. M., Gonzales, M., Herron, G. S., Nagavarapu, U., Hopkinson, S. B., Tsuruta, D. and Jones, J. C. (2002). Complex interactions between the laminin alpha 4 subunit and integrins regulate endothelial cell behavior in vitro and angiogenesis in vivo. *Proc. Natl. Acad. Sci. USA* **99**, 16075-16080.

Hixenbaugh, E. A., Goeckeler, Z. M., Papaiya, N. N., Wysolmerski, R. B., Silverstein, S. C. and Huang, A. J. (1997). Stimulated neutrophils induce myosin light chain phosphorylation and isometric tension in endothelial cells. *Am. J. Physiol.* **273**, H981-H988.

Ingber, D. E. and Folkman, J. (1989a). How does extracellular matrix control capillary morphogenesis? *Cell* **58**, 803-805.

Ingber, D. E. and Folkman, J. (1989b). Mechanochemical switching between growth and differentiation during fibroblast growth factor-stimulated angiogenesis in vitro: role of extracellular matrix. *J. Cell Biol.* **109**, 317-330.

Kamei, M., Saunders, W. B., Bayless, K. J., Dye, L., Davis, G. E. and Weinstein, B. M. (2006). Endothelial tubes assemble from intracellular vacuoles in vivo. *Nature* **442**, 453-456.

Kamm, K. E. and Stull, J. T. (2001). Dedicated myosin light chain kinases with diverse cellular functions. *J. Biol. Chem.* **276**, 4527-4530.

Kedrin, D., Gligorijevic, B., Wyckoff, J., Verkhusha, V. V., Condeelis, J., Segall, J. E. and van Rheenen, J. (2008). Intravital imaging of metastatic behavior through a mammary imaging window. *Nat. Methods* **5**, 1019-1021.

Korff, T. and Augustin, H. G. (1999). Tensional forces in fibrillar extracellular matrices control directional capillary sprouting. *J. Cell Sci.* **112 (Pt 19)**, 3249-3258.

Li, H., Fan, X. and Houghton, J. (2007). Tumor microenvironment: the role of the tumor stroma in cancer. *J. Cell Biochem.* **101**, 805-815.

Lorenzon, P., Vecile, E., Nardon, E., Ferrero, E., Harlan, J. M., Tedesco, F. and Dobrina, A. (1998). Endothelial cell E- and P-selectin and vascular cell adhesion molecule-1 function as signaling receptors. *J. Cell Biol.* **142**, 1381-1391.

Lunt, S. J., Chaudary, N. and Hill, R. P. (2008). The tumor microenvironment and metastatic disease. *Clin. Exp. Metastasis*. **26**, 19-34.

Mierke, C. T., Rosel, D., Fabry, B. and Brabek, J. (2008a). Contractile forces in tumor cell migration. *Eur. J. Cell Biol.* **87**, 669-676.

Mierke, C. T., Zitterbart, D. P., Kollmannsberger, P., Raupach, C., Schlotzer-Schrehardt, U., Goecke, T. W., Behrens, J. and Fabry, B. (2008b). Breakdown of the endothelial barrier function in tumor cell transmigration. *Biophys. J.* **94**, 2832-2846.

Millan, J., Hewlett, L., Glyn, M., Toomre, D., Clark, P. and Ridley, A. J. (2006). Lymphocyte transcellular migration occurs through recruitment of endothelial ICAM-1 to caveola- and F-actin-rich domains. *Nat. Cell Biol.* **8**, 113-123.

Miyawaki, A., Llopis, J., Heim, R., McCaffery, J. M., Adams, J. A., Ikura, M. and Tsien, R. Y. (1997). Fluorescent indicators for Ca2+ based on green fluorescent proteins and calmodulin. *Nature* **388**, 882-887.

Montesano, R. and Orci, L. (1988). Intracellular diaphragmed fenestrae in cultured capillary endothelial cells. *J. Cell Sci.* **89 (Pt 3)**, 441-447.

Montesano, R., Pepper, M. S., Vassalli, J. D. and Orci, L. (1987). Phorbol ester induces cultured endothelial cells to invade a fibrin matrix in the presence of fibrinolytic inhibitors. *J. Cell Physiol.* **132**, 509-516.

Nakatsu, M. N., Sainson, R. C., Aoto, J. N., Taylor, K. L., Aitkenhead, M., Perez-del-Pulgar, S., Carpenter, P. M. and Hughes, C. C. (2003). Angiogenic sprouting and capillary lumen formation modeled by human umbilical vein endothelial cells (HUVEC) in fibrin gels: the role of fibroblasts and Angiopoietin-1. *Microvasc. Res.* **66**, 102-112.

Nicosia, R. F., Tchao, R. and Leighton, J. (1982). Histotypic angiogenesis in vitro: light microscopic, ultrastructural, and radioautographic studies. *In Vitro* **18**, 538-549.

Nieminen, M., Henttinen, T., Merinen, M., Marttila-Ichihara, F., Eriksson, J. E. and Jalkanen, S. (2006). Vimentin function in lymphocyte adhesion and transcellular migration. *Nat. Cell Biol.* **8**, 156-162.

Parkhurst, M. R. and Saltzman, W. M. (1992). Quantification of human neutrophil motility in three-dimensional collagen gels. Effect of collagen concentration. *Biophys. J.* **61**, 306-315.

Stull, J. T., Bowman, B. F., Gallagher, P. J., Herring, B. P., Hsu, L. C., Kamm, K. E., Kubota, Y., Leachman, S. A., Sweeney, H. L. and Tansey, M. G. (1990). Myosin phosphorylation in smooth and skeletal muscles: regulation and function. *Prog. Clin. Biol. Res.* **327**, 107-126.

Totsukawa, G., Yamakita, Y., Yamashiro, S., Hartshorne, D. J., Sasaki, Y. and Matsumura, F. (2000). Distinct roles of ROCK (Rho-kinase) and MLCK in spatial regulation of MLC phosphorylation for assembly of stress fibers and focal adhesions in 3T3 fibroblasts. *J. Cell Biol.* **150**, 797-806.

Verin, A. D., Patterson, C. E., Day, M. A. and Garcia, J. G. (1995). Regulation of endothelial cell gap formation and barrier function by myosin-associated phosphatase activities. *Am. J. Physiol.* **269**, L99-L108.

Wiche, G. (1998). Role of plectin in cytoskeleton organization and dynamics. *J. Cell Sci.* **111 (Pt 17)**, 2477-2486.

Wittchen, E. S., van Buul, J. D., Burridge, K. and Worthylake, R. A. (2005). Trading spaces: Rap, Rac, and Rho as architects of transendothelial migration. *Curr. Opin. Hematol.* **12**, 14-21.

Witz, I. P. (2006). Tumor-microenvironment interactions: the selectin-selectin ligand axis in tumor-endothelium cross talk. *Cancer Treat Res.* **130**, 125-140.

Witz, I. P. (2008). Yin-yang activities and vicious cycles in the tumor microenvironment. *Cancer Res.* **68**, 9-13.

Wolff, J. R. and Bar, T. (1972). 'Seamless' endothelia in brain capillaries during development of the rat's cerebral cortex. *Brain Res.* **41**, 17-24.

Worthylake, R. A., Lemoine, S., Watson, J. M. and Burridge, K. (2001). RhoA is required for monocyte tail retraction during transendothelial migration. *J. Cell Biol.* **154**, 147-160.

Wysolmerski, R. B. and Lagunoff, D. (1990). Involvement of myosin light-chain kinase in endothelial cell retraction. *Proc. Natl. Acad. Sci. USA* **87**, 16-20.

Wysolmerski, R. B. and Lagunoff, D. (1991). Regulation of permeabilized endothelial cell retraction by myosin phosphorylation. *Am J. Physiol.* **261**, C32-C40.

Youvan, D. C., Silva, C. M., Bylina, E. J., Coleman, W. J., Dilworth, M. R. and Yang, M. M. (1997). Calibration of fluorescence resonance energy transfer in microscopy using genetically engineered GFP derivatives on nickel chelating beads. *Biotechnology et alia* **3**, 1-18.

Zeng, Q., Lagunoff, D., Masaracchia, R., Goeckeler, Z., Cote, G. and Wysolmerski, R. (2000). Endothelial cell retraction is induced by PAK2 monophosphorylation of myosin II. *J. Cell Sci.* **113**, 471-482.

Zijlstra, A., Lewis, J., Degryse, B., Stuhlmann, H. and Quigley, J. P. (2008). The inhibition of tumor cell intravasation and subsequent metastasis via regulation of in vivo tumor cell motility by the tetraspanin CD151. *Cancer Cell* **13**, 221-234.